Polysulfide Shuttle Study in the Li/S Battery System

Journal of The Electrochemical Society, **151** (11) A1969-A1976 (2004)
0013-4651/2004/151(11)/A1969/8/$7.00 © The Electrochemical Society, Inc.

Polysulfide Shuttle Study in the Li/S Battery System

Yuriy V. Mikhaylik*,z and James R. Akridge*

Sion Power Corporation, Tucson, Arizona 85747-9108, USA

This work reports a quantitative analysis of the shuttle phenomenon in Li/S rechargeable batteries. The work encompasses theoretical models of the charge process, charge and discharge capacity, overcharge protection, thermal effects, self-discharge, and a comparison of simulated and experimental data. The work focused on the features of polysulfide chemistry and polysulfide interaction with the Li anode, a quantitative description of these phenomena, and their application to the development of a high-energy rechargeable battery. The objective is to present experimental evidence that self-discharge, charge-discharge efficiency, charge profile, and overcharge protection are all facets of the same phenomenon.
 [DOI: 10.1149/1.1806394]

Manuscript submitted November 14, 2003; revised manuscript received April 2, 2004. Available electronically October 27, 2004.

The Gibbs energy of the Li/S reaction is about 2600 Wh/kg, more than five times the theoretical energy of a Li-ion system. During last three decades, there has been a strong incentive to develop a rechargeable Li/S battery. Two approaches have been explored to incorporate sulfur into the cell: creating the cathode with solid elemental sulfur, and employing an electrolyte with sulfur completely dissolved in the form of polysulfides Li_2S_x. The pioneering work of Rauh[1] showed that electrolyte systems based on solvents with high basicity could dissolve a large amount of lithium polysulfides. In dimethyl sulfoxide or ethers like tetrahydrofuran,[2] the sulfur solubility as Li_2S_x can exceed 10 M. Spectroscopic and electrochemical studies of polysulfides in nonaqueous solutions suggest that their dynamic equilibrium, redox chemistry, and kinetics are strongly affected by solvent complexation.[1,2] Further exploration of high sulfur solubility electrolytes involved dioxolane[3] and glyme solvents[4-6] as more practical for rechargeable Li/S systems. High polysulfide solubility electrolytes enable the Li/S battery to operate as a liquid cathode system no matter how the starting sulfur active material was incorporated into the cell, solid as S_8 or liquid as polysulfides. Batteries with a liquid polysulfide cathode demonstrate a high rate capability and a wide range of operating temperatures.[7,8] Soluble polysulfides as well as soluble sulfur cause lithium corrosion and, because of their relatively high mobility, they create a polysulfide shuttle phenomenon during the battery charge process. There are few papers connecting the shuttle phenomenon with Li/S cell performance characteristics. The papers published describe the shuttle mainly in a qualitative manner.[3,5,7,9] There are no publications that connect Li/S battery self-discharge, charge-discharge efficiency, discharge capacity, and overcharge protection in a quantitative manner.

Experimental

Cathodes containing elemental sulfur, acetylene black, graphite, and a binder cross-linkable at elevated temperatures were coated on an aluminized poly(ethylene terephthalate) (PET) substrate. The cathode slurry preparation and coating procedure are described by Cheng.[10] The PET film was 6 μm thick. The aluminum layer thickness was ~500 Å, and the total cathode thickness was 70 μm (double-sided coated measurement). A 50 μm thick lithium foil was used as the anode. The cathode, anode, and a porous polyolefin separator were combined into a layered structure of cathode/separator/anode that was wound and compressed, with the liquid electrolyte filling the void areas of the separator and cathode to form prismatic cells with an electrode area of about 840 cm^2. The electrolytes were solutions of lithium bis(trifluoromethylsulfonyl)imide $LiN(CF_3SO_2)_2$ in a 40:55 volume ratio mixture of 1,3-dioxolane (DOL) and 1,2-dimethoxyethane (DME). Three lithium salt concentrations, 0.5, 1.85, and 2.5 *m*, were applied to make electrolytes 1, 2, and 3. All cells contained ~1 g of sulfur and ~4 mL of electrolyte. The total cell weight was ~10 g. After sealing the cells in a foil pouch, they were subjected to electrical test. Electrical testing was performed with a Digatron multiple battery tester MBT 01-05-16.

Discharge Profile at Room Temperature

Typical ambient Li/S cell discharge curves consist of two plateaus.[1,3,5,7] During the first discharge, molecules of elemental sulfur (S_8) accept electrons, generating a chain of lithium polysulfides (Li_2S_x). Usually polysulfides with $x \sim 6$-8 are generated at a high voltage plateau (2.3-2.4 V), and further polysulfide reduction takes place at a low voltage plateau (~2.1 V). Our prismatic cell experimental data shows that the first discharge corresponds to accepting 0.5 electron per one atom of sulfur at the high voltage plateau. The low discharge voltage plateau indicates acceptance of an additional one electron per sulfur atom (Fig. 1).

Acceptance of 0.5 electron per sulfur atom at the high discharge plateau reduces cyclo-octasulfur molecules S_8 as the starting cathode material to lithium tetrasulfide Li_2S_4. The electrochemical reaction and the Nernst equation corresponding to this process are

$$S_8^0 + 4e^- = 2S_4^{2-} \quad [1]$$

$$E_H = E_H^O + \frac{RT}{n_H F} \ln \frac{[S_8^0]}{[S_4^{2-}]^2} \quad [2]$$

Acceptance of 0.5 electron per sulfur atom also could be interpreted to mean that the high plateau sulfur S_H is represented by S_8 and all forms of polysulfides S_x^{2-} with $x > 4$. Based on Eq. 1, the high plateau sulfur specific capacity q_H is 419 mAh/g.

The low discharge plateau process, involving acceptance of an additional electron per sulfur atom, is the reduction of lithium tetrasulfide, which generates a lithium sulfide and disulfide mixture. The low plateau reaction and Nernst equation are

$$S_4^{2-} + 4e^- = 2S^{2-} + S_2^{2-} \quad [3]$$

$$E_L = E_L^O + \frac{RT}{n_L F} \ln \frac{[S_4^{2-}]}{[S^{2-}]^2[S_2^{2-}]} \quad [4]$$

Practical discharge stops at this point due to lithium disulfide's low solubility in the electrolyte solvents and its very slow electrochemical kinetics. Acceptance of one electron per sulfur atom also could be interpreted to mean that the low plateau sulfur S_L is represented by all forms of polysulfides S_x^{2-} with $x < 4$. Based on Eq. 3, the low plateau sulfur specific capacity q_L is 837 mAh/g. The total experimentally accessible high and low plateau specific capacity is 1.5 electron per sulfur atom or ~1256 mAh per gram of sulfur. Acceptance of 1.5 electron in the DME/DOL mixture is close to obtained in tetrahydrafuran-based electrolyte[1] at a C/50 discharge rate. It should be mentioned that the sulfur specific capacity of 1256 mAh/g typically could be achieved only for the first discharge of the fresh cell. For the cells with an unprotected lithium anode, the fur-

* Electrochemical Society Active Member.
z E-mail: yuriy.mikhaylik@sionpower.com

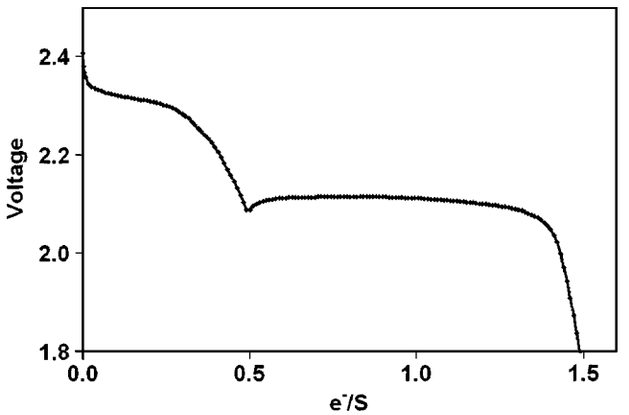

Figure 1. Experimental first discharge profile at C/30 rate for cell with 1.85 *m* $LiN(CF_3SO_2)_2$.

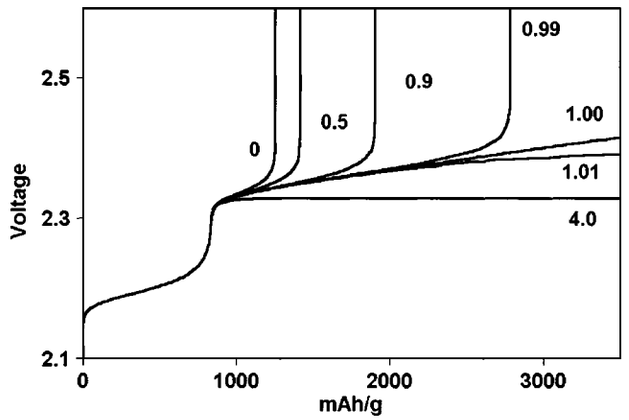

Figure 2. Simulated charge profiles at different $k_s q_H[S_{total}]/I_C$ factors.

ther charge does not recover all capacity because of the polysulfide shuttle. This phenomenon is analyzed in more detail.

The discharge profile analysis (Fig. 1) at low discharge currents when the cell polarization is negligible as well as open-circuit voltage measurements allowed us to estimate the high and low plateau standard potentials of $E^0_H = 2.33$ V and $E^0_L = 2.18$ V.

Charge and Shuttle Equation

The first recharge of a Li/S cell does not result in the polysulfides transforming into elemental sulfur. During the second and following charges, the higher-order polysulfides, which are generated at the ''sulfur'' electrode during the latter stages of the charge, diffuse to the lithium electrode where they react directly with the lithium in a parasitic reaction to recreate the lower-order polysulfides. These species diffuse back to the sulfur electrode to generate the higher forms of polysulfide again, thus creating a shuttle mechanism. If the rate of reduction of high polysulfides on the Li anode surface is directly proportional to their concentration $[S_H]$, the total high plateau polysulfide dynamic could be expressed with the following differential equation (Eq. 5) including charge-discharge current and shuttle phenomena

$$\frac{d[S_H]}{dt} = \frac{I}{q_H} - k_s[S_H] \quad [5]$$

$[S_H]$ is a high polysulfide amount or concentration normalized to a certain cell volume or surface, t is the time, I is the charge or discharge current normalized to a certain surface or volume, q_H is the sulfur specific capacity related to the high voltage plateau, and k_s is the heterogeneous reaction constant or shuttle constant.

The value of current is positive, $I = I_C$, for the charge process and negative for the discharge process, $I = -I_D$.

The general solution of the differential equation (Eq. 5) is

$$\frac{I - q_H k_s[S_H]}{I - q_H k_s[S^0_H]} = e^{-k_s t} \quad [6]$$

$[S^0_H]$ is a high plateau polysulfide concentration at $t = 0$.

If the charge started at fully discharged conditions when $[S^0_H] = 0$, the high polysulfide concentration could be expressed with Eq. 7

$$[S_H] = \frac{I_C}{k_s q_H}(1 - e^{-kt_C}) \quad [7]$$

t_C is the charge time at the high plateau. Equation 7 is an integral form of the charge-shuttle equation (Eq. 5).

Charge Profile and Shuttle

The high and low plateau Nernst equations (Eq. 1 and 3) combined with the shuttle equation (Eq. 7) permit the generation of cell charge profiles. To do this, three additional conditions related to the high and low plateau charge processes are considered. The first relates to sulfur material balance and is represented by Eq. 8. Equation 8 says that the sum of all forms of polysulfide and sulfur always equals the total amount of sulfur in the cell

$$[S_{total}] = \sum x[S_x] \quad [8]$$

The second condition is charge balance, and it requires that polysulfides at the high and low plateau generate the whole cell accumulated capacity. This capacity Q_{ac} is presented by Eq. 9

$$Q_{ac} = [S_H](q_H + q_L) + [S_L]q_L \quad [9]$$

The third condition relates to continuity of the charge-discharge curve and says that all polysulfides on high and low plateaus are in equilibrium. This condition is expressed by Eq. 10

$$E^O_H + \frac{RT}{n_H F}\ln\frac{[S^0_8]}{[S^{2-}_4]^2} = E^O_L + \frac{RT}{n_L F}\ln\frac{[S^{2-}_4]}{[S^{2-}]^2[S^{2-}_2]} \quad [10]$$

Based on Eq. 1, 3, 7, and 8-10, charge profiles at various values of charge current and shuttle constant were generated. To simplify the analysis, ohmic, interfacial charge transfer, and diffusion cell polarization were not considered. The cell voltage included only concentration polarization based on Nernst equations. It was also assumed that the charge efficiency at the low plateau was 100%, indicating very slow Li corrosion with low polysulfides. The charge profiles generated are shown in Fig. 2. There are two different charge behaviors depending on the ratio of charge current I_c, high plateau sulfur specific capacity q_H, total sulfur concentration $[S_{total}]$, and shuttle constant k_s. This ratio is represented by the charge-shuttle Factor (f_C)

$$\frac{k_s q_H[S_{total}]}{I_C} = f_C \quad [11]$$

At $k_s q_H[S_{total}]/I_C < 1$, when the charge current is high enough or the shuttle constant is low, the cell could be charged completely, showing a sharp voltage increase. At $k_s q_H[S_{total}]/I_C > 1$, the cell never reaches complete charge and shows a voltage leveling. The larger the value of f_C, the lower the leveled voltage. Charging at these conditions could proceed infinitely, demonstrating high overcharge protection. The criteria of overcharge protection is I_C

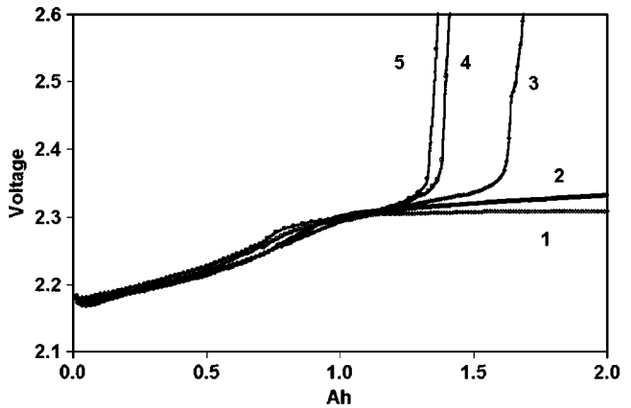

Figure 3. Experimental charge profiles at different currents for cell with 1.85 *m* $LiN(CF_3SO_2)_2$: (1) 20 mA, $f_C = 4$; (2) 50 mA, $f_C = 1.6$; (3) 100 mA, $f_C = 0.8$; (4) 200 mA, $f_C = 0.4$; (5) 400 mA, $f_C = 0.2$.

$< k_s q_H[S_{total}]$. When f_C is exactly equal to 1, the high plateau charge process is represented by a linearly increasing voltage curve (Fig. 2). However, it is unlikely for the conditions to be stable for the entire charge process. Minor fluctuations of temperature due to cell self-heating could slightly increase the shuttle constant and move the voltage curve down. The curves with f_C equal to 0.99, 1.00, and 1.01 in Fig. 2 show that small differences can cause dramatic changes in the charge profiles. This phenomenon is analyzed in more detail.

Experimental charge profiles corrected for IR-drop are presented in Fig. 3 and 4. The experimental charge profiles in Fig. 3 and 4 represent spectra of charge-shuttle factors, exceeding 1 and significantly below 1, with a sharp voltage increase and with voltage leveling. The whole range of experimental charge-shuttle factors was generated in two ways: with the shuttle constant fixed and varying the charge currents, and with the charge current fixed and applying different electrolytes and shuttle constants. Figure 3 represents the cells with the same electrolyte and the same shuttle constant but charged at different currents. Figure 4 represents the cells charged at constant current but with different electrolytes and shuttle constants. The estimation of shuttle constants and charge-shuttle factors is described in the next section. Generally, the shuttle constant is a function of the electrolyte component's chemical properties and concentration. All charge profiles in Fig. 3 relate to cells with the same electrolyte, *i.e.*, 1.85 *m* salt, meaning that the shuttle constant for these cells was the same. The cells were charged at currents in the range from 20-400 mA, giving f_C values greater and lower than 1. Figure 4 represents charge profiles at a constant charge current of 200 mA. The salt concentration in the electrolyte was varied from 0.5 to 2.5 *m* in a mixture of DOL and DME. The salt concentration increase from 0.5 to 2.5 m allowed reduction of the shuttle constant and allowed us to obtain f_C values above and below 1 at constant charge current. Both Fig. 3 and 4 demonstrated good agreement between the simulated (Fig. 2) and experimental data.

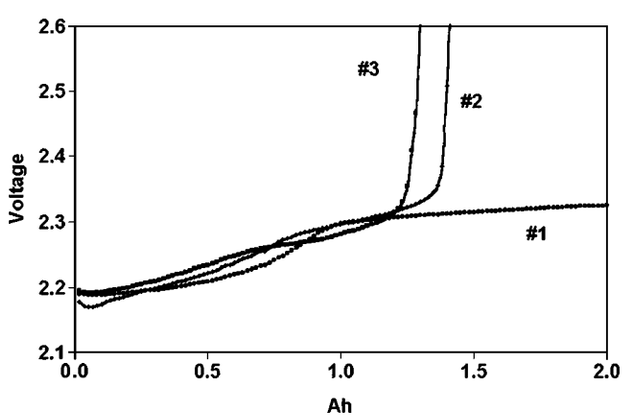

Figure 4. Experimental charge profiles at 200 mA charge current for cells with different $LiN(CF_3SO_2)_2$ salt concentrations: (#1) 0.5 *m*, $f_C = 1.11$; (#2) 1.85 *m*, $f_C = 0.4$; (#3) 2.5 *m*, $f_C = 0.21$.

Shuttle, Accumulated Capacity, and Overcharge

The high plateau accumulated capacity Q_H^{acc} is proportional to the amount of generated high plateau polysulfides $[S_H]$ and the high plateau sulfur specific capacity q_H. The value of $[S_H]$ can be estimated using Eq. 7. At constant current and charge time (t_C), the high plateau accumulated capacity can be derived from Eq. 12

$$Q_H^{acc} = [S_H]q_H = \frac{I_C}{k_s}(1 - e^{-k/t}) \quad [12]$$

The shuttle phenomenon reduces the charge efficiency at the high plateau. For charge-shuttle factors higher than 0 but below 1, an overcharge is needed to reach complete polysulfide oxidation into elemental sulfur. At complete polysulfide oxidation, a sharp voltage increase on the charge curve could be observed (Fig. 2-4). Under these conditions, high plateau sulfur $[S_H]$ reaches its maximal value equal to the total amount of sulfur in the cell $[S_{total}]$. The maximal high plateau charge time corresponding to full conversion of polysulfide into elemental sulfur can be found from Eq. 13

$$t_C^{max} = -\frac{1}{k_S}\ln\left(1 - \frac{q_H k_S[S_{total}]}{I_C}\right) \quad [13]$$

The applied high plateau charge capacity is simply proportional to the charge time

$$Q_H^{applied} = I_C t_C \quad [14]$$

The high plateau overcharge corresponding to these conditions can be found as a relative difference between the applied and accumulated capacity (Eq. 15)

$$H_{OC} = \frac{Q_H^{applied} - Q_H^{acc}}{Q_H^{acc}} = \frac{k_s t_C}{1 - e^{-k/t}} - 1 \quad [15]$$

For charge-shuttle factors below 1, the maximal charge time is finite, and the overcharge is limited by this time. When $t_C = t_C^{max}$, the overcharge can be expressed by Eq. 16

$$H_{OC} = -\frac{1}{f_C}\ln(1 - f_C) - 1 \quad [16]$$

For full charge conditions, the high plateau overcharge is a simple function of the charge-shuttle factor. The overcharge simulation based on Eq. 16 is presented in Fig. 5

At a charge-shuttle factor between 0.1-0.2, an insignificant overcharge is needed to reach full charge conditions. At higher values of f_C corresponding to higher values of the shuttle constant or lower charge currents, the overcharge could exceed 100%. The closer to 1 the value of the charge-shuttle factor, the higher the overcharge needed for complete charge. When the f_C factor exceeds 1, the high polysulfides are never completely converted into elemental sulfur, regardless of how long the charge proceeds. For long charge times when $k_S t_C \gg 1$, Eq. 12 for the accumulated high plateau capacity can be simplified

$$Q_H = [S_H]q_H = \frac{I_C}{k_s} \quad [17]$$

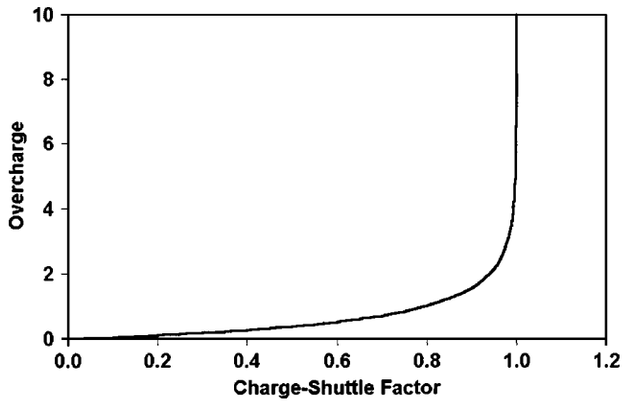

Figure 5. High plateau overcharge as a function of charge-shuttle factor.

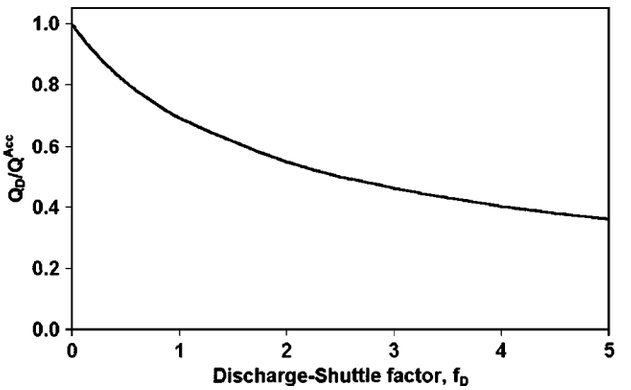

Figure 6. Relative high plateau discharge capacity as function of discharge-shuttle factor.

Under these conditions, at very effective shuttle or very low charge currents, the high plateau accumulated capacity is directly proportional to the charge current but is still below its maximal value $q_H[S_{total}]$.

In the region of very low charge currents, a simple experimental method of shuttle constant estimation exists. The first derivative of the high plateau capacity gives the reciprocal value of the shuttle constant

$$\frac{dQ_H}{dI_C} = \frac{1}{k_S} \quad [18]$$

Discharge Capacity as a Function of Discharge Current

The experimental high plateau discharge capacity Q_D^H is not always equal to the accumulated capacity. When the discharge process starts, two parallel paths exist for high polysulfide reduction: first simple electrochemical reduction due to the discharge current, and second, reduction of polysulfides on the Li anode that depends on the shuttle constant (Eq. 5).

If a discharge process at current I_D starts immediately after charge, the beginning amount of high plateau polysulfides $[S_H^0]$ and accumulated capacity can be found from Eq. 12 describing the charge process. Equation 6 with a negative value for the current represents a discharge process started at $[S_H^0]$ and accompanied with a shuttle. The discharge time t_D corresponding to reduction of high polysulfide concentration from starting level $[S_H^0]$ to 0 resulting from the preceding processes can be derived from Eq. 19

$$t_D = \frac{1}{k_s}\ln\left(1 + \frac{k_s q_H [S_H^0]}{I_D}\right) \quad [19]$$

Finally, the high plateau discharge capacity as a function of discharge current is presented by Eq. 20

$$Q_D^H = I_D t_D = \frac{I_D}{k_s}\ln\left(1 + \frac{k_s q_H [S_H^0]}{I_D}\right) \quad [20]$$

Equation 20 can be transformed into a simpler form

$$Q_D^H = Q_H^{acc}\frac{\ln(1 + f_D)}{f_D} \quad [21]$$

where the charge accumulated capacity is

$$Q_H^{acc} = [S_H^0] q_H \quad [22]$$

and f_D is the discharge-shuttle factor

$$f_D = \frac{k_S Q_H^{acc}}{I_D} \quad [23]$$

The discharge capacity Q_D from Eq. 20 and 21 can be measured experimentally. Analysis of Eq. 21 shows that the high plateau discharge capacity can reach its maximal value equal to the charge accumulated capacity only when the discharge-shuttle factor is close to zero. More than 90% of the accumulated capacity could be gained at f_D below 0.2. Experimentally, such conditions could be reached at a high enough discharge current or a low shuttle constant. On the opposite side of the experimental conditions, at very low discharge currents, the shuttle has enough time to significantly reduce the discharge capacity. Under these conditions, the experimental high plateau discharge capacity must be significantly lower than the accumulated charge capacity. The simulation presented in Fig. 6 shows the discharge capacity as a fraction of accumulated capacity for a wide range of discharge-shuttle factors.

Generally, for the wide range of discharge currents, the high plateau capacity must increase from zero at very low currents and then reach a leveling maximum corresponding to the charge accumulated capacity.

An experimental evaluation of discharge current influence on high plateau capacity was performed with cells containing 0.5, 1.85, and 2.5 *m* salt electrolytes. The cells were charged at a constant current of 200 mA to a voltage of 2.8 V if the charge process showed a sharp voltage increase (1.85 and 2.5 m salt concentrations) or to a total charge capacity of 2000 mAh if the cell showed voltage leveling. The cells were subjected to discharge immediately after

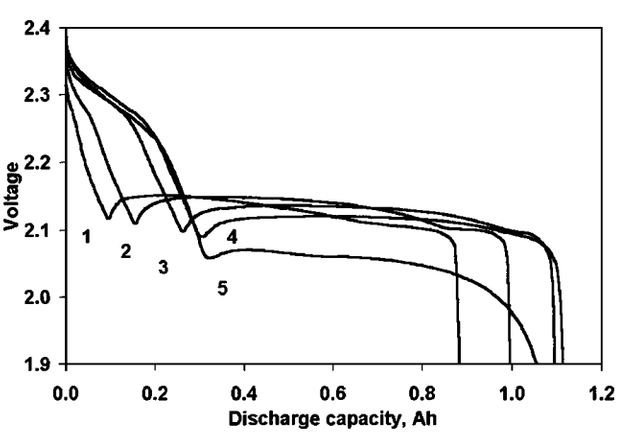

Figure 7. Cell discharge profiles for cell with 1.85 m $LiN(CF_3SO_2)_2$ at different current values: (1) 10, (2) 20, (3) 50, (4) 100, and (5) 350 mA.

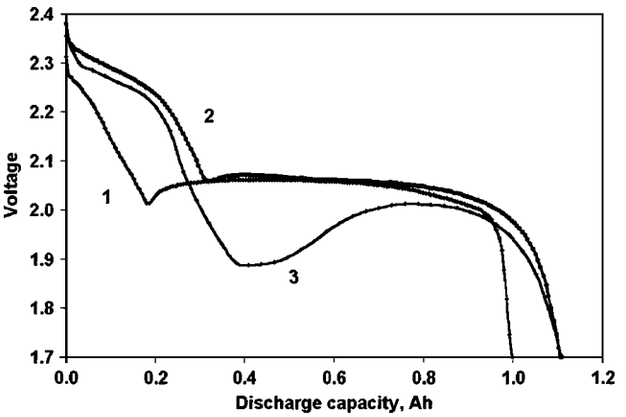

Figure 8. Discharge profiles at 350 mA discharge current for cells with different salt concentrations: (1) 0.5, (2) 1.85, and (3) 2.5 *m*.

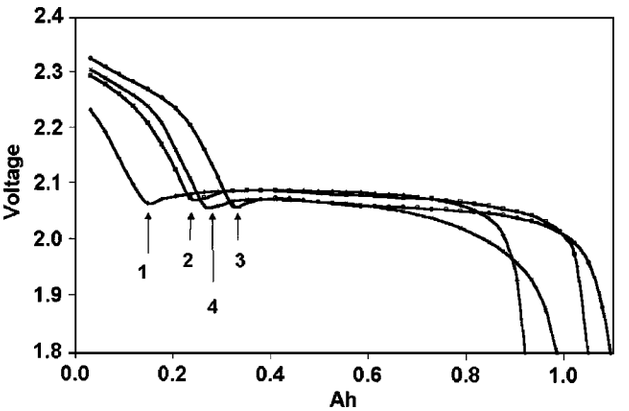

Figure 10. Experimental discharge profiles for cell with 1.85 *m* $LiN(CF_3SO_2)_2$ electrolyte. Discharge 350 mA. Charge current: (1) 20, (2) 50, (3) 200, and (4) 800 mA.

charge at currents from 10 to 1000 mA. Figure 7 represents selected discharge profiles at different discharge currents for cells with 1.85 m salt electrolyte. Figure 8 represents discharge profiles at constant discharge current 350 mA for cells with three different electrolytes. The high plateau discharge capacity was extracted from the discharge profiles and plotted *vs.* discharge current in Fig. 9.

Generally all experimental data in Fig. 9 follow the theoretical lines based on Eq. 20-23. The different maximal capacity leveling values for 0.5, 1.85, and 2.5 *m* salt concentration electrolytes correspond to different charge efficiencies and, as a result, different accumulated charge capacities. The high plateau discharge capacity reached its maximal value at a discharge current equal to or exceeding 350 mA for all tested electrolytes. This discharge current was applied for experimental evaluation of charge current influence on high plateau capacity.

Discharge Capacity as a Function of Charge Current

Experimental evaluation of the high plateau discharge capacity at different charge currents has been performed at a constant discharge current of 350 mA and at charge currents in the range of 20-1000 mA. The cells with 0.5, 1.85, and 2.5 *m* salt concentration in a mixture of DOL and DME were charged to 2.8 V provided the charge process showed a sharp voltage increase or to a total charge capacity of 2000 mAh if the cell showed voltage leveling. As an example, Fig. 10 represents experimental discharge profiles for a cell with 1.85 *m* salt concentration electrolyte after charge at different currents.

The high plateau discharge capacity was extracted from experimental discharge profiles and plotted *vs.* charge current in Fig. 11. Theoretical curves are also presented in this figure. The values of k_S for simulation were obtained in the range of low charge currents where the high plateau discharge capacity was linearly proportional to the charge current (Eq. 18). A shuttle constant corresponding to the charge process for the three tested electrolytes has been used for simulation of high plateau discharge capacity for the total range of applied charge currents based on Eq. 12. The inflection point on the simulated curves corresponds to the transition from charge with leveling voltage ($f_C > 1$) to sharp voltage increase ($f_C < 1$).

Simulations are in agreement with experimental data for the full range of charge currents for the cells with 2.5 *m* salt concentration in a DOL and DME mixture and relatively low shuttle constant. However, for lower concentration electrolytes and higher values of the shuttle constant, the experimental data showed a substantially lower high plateau capacity compared with theory. The differences increased with higher charge currents. This means the shuttle constant at the high charge currents was bigger compared with that at low

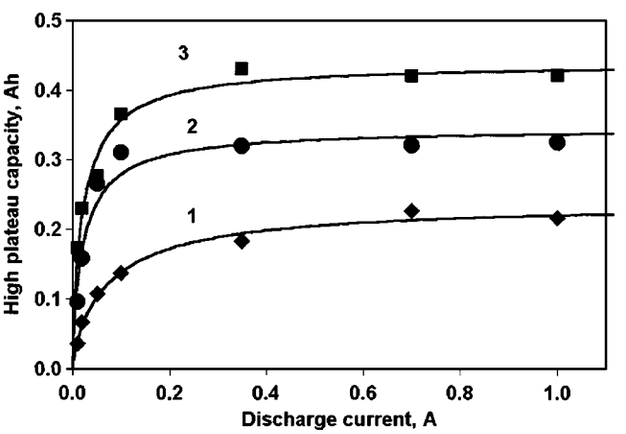

Figure 9. High plateau capacity as a function of discharge current for cells with different salt concentration electrolytes: (1) 0.5 *m*, ♦ is experimental data, line is simulation at $k_S = 0.45\ h^{-1}$; (2) 1.85 m, ● is experimental data, line is simulation at $k_S = 0.14\ h^{-1}$; (3) 2.5 *m*, ■ is experimental data, line is simulation at $k_S = 0.095\ h^{-1}$.

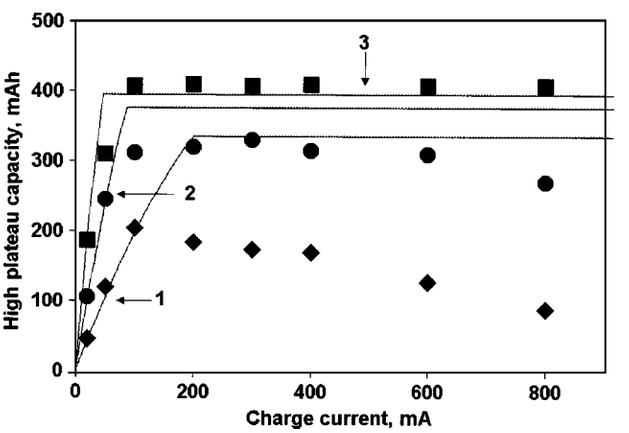

Figure 11. High plateau capacity as a function of charge current for cells with different $LiN(CF_3SO_2)_2$ salt concentrations in 40:55 volume ratio mixture of DOL and DME electrolytes: (1) 0.5 *m*, ♦ is experimental data, line is simulation at $k_S = 0.53\ h^{-1}$; (2) 1.85 *m*, ● is experimental data, line is simulation at $k_S = 0.19\ h^{-1}$; (3) 2.5 *m*, ■ is experimental data, line is simulation at $k_S = 0.10\ h^{-1}$.

Table I. Model parameters.

Parameter	Symbol	Value
High plateau sulfur specific capacity	q_H	419 mAh/g
Low plateau sulfur specific capacity	q_L	837 mAh/g
High plateau standard potential	E^0_H	2.33 V
Low plateau standard potential	E^0_L	2.18 V
Total sulfur mass in the cell	S_{total}	1 g
Cells mass	m	10 g
Cell heat-transfer coefficient	α	0.038 W K^{-1}
Cell heat capacity	c_h	1.65 J g^{-1} K^{-1}
Shuttle activation energy	A	0.56 eV

current conditions. The capacity decrease could be explained by a cell self-heating phenomenon. It was shown that the shuttle triggered cell self-heating at high plateau charge.[7] The higher the shuttle constant, the higher is the current fraction leading to self-heating. A higher cell internal temperature increases the rate of polysulfide reaction with the lithium anode and the shuttle constant, respectively. This positive feedback relation between shuttle constant, charge current, and internal temperature leads to lower accumulated and discharge capacity.

Shuttle and Cell Self-Heating

Cell self-heating increases the rate of polysulfide interaction with the lithium anode and leads to an increase of the shuttle constant. Typically, a charge process starts when the cell is at temperature T_0 with shuttle constant $k_S(T_0)$. At the end of charge, the cell internal temperature increases to T, and the shuttle constant at this point is represented by an Arrhenius (Eq. 24)

$$k_S(T) = k(T_0)\exp\left[-\frac{A}{R}\left(\frac{1}{T} - \frac{1}{T_0}\right)\right] \quad [24]$$

where A is the shuttle activation energy.

If the charge time is long enough, the cell can reach heat steady-state conditions. At this point, internal heat generation is equal to the heat dissipated due to the temperature gradient. The following equation represents the steady-state conditions

$$I_C V_H = \alpha(T - T_0) \quad [25]$$

The left side of Eq. 25 represents the internal heat generation as proportional to the shuttle current and high plateau voltage. The right side of 25 is heat dissipation in which α is the cell heat transfer coefficient.

If the charge proceeds long enough and shows voltage leveling, the accumulated capacity can be derived from Eq. 17, taking into account the changing shuttle constant (Eq. 24) and heat balance (Eq. 25). Accumulated capacity simulation based on Eq. 17, 24, 26 and the model parameters in Table I, as well as experimental data are presented in Fig. 12. The experimental high plateau capacity was taken from 0.5 m salt concentration in DOL and DME electrolyte cells discharged at 350 mA. These cells consistently showed voltage leveling for the range of charge currents, thus allowing application of Eq. 17. At these conditions, the whole electrode stack was considered as a lumped mass with uniform temperature T. Consideration of self-heating effects leads to much better agreement between the theoretical and experimental data (Fig. 12) *vs.* simulations for isothermal conditions (Fig. 11).

It was shown[7] that the applied cell design could reach thermal steady-state conditions during times exceeding ~15 min. This time corresponds to a heat transfer factor $\alpha \sim 0.08$ W K^{-1} and could be achieved under force convection conditions. Without force convection, the heat transfer coefficient is lower, ~0.038 W K^{-1} (Fig. 12). Under these conditions, heat dissipation proceeds slowly and requires a longer time. If the heat transfer is stalled significantly, the time corresponding to establishment of thermal equilibrium could be

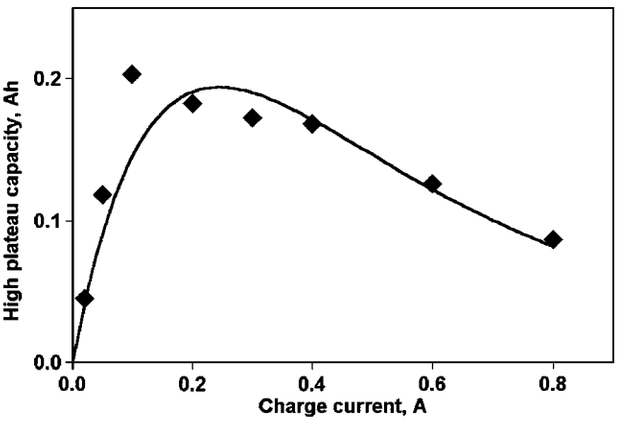

Figure 12. Simulated and experimental high plateau capacity *vs.* charge current. Simulation parameters: $k_S(T_0) = 0.53$ h^{-1}, $T_0 = 298$ K, $A = 0.56$ eV, and $\alpha = 0.038$ W K^{-1}.

comparable with the total charge time. In this case, the high plateau voltage could pass through a maximum. This would be a rare event, because it requires specific and very narrow combinations of charge and heat dissipation parameters. Figure 13 demonstrates the charge profile for the cell placed in a polyethylene bag. The bag reduced the heat dissipation rate by a factor of ~2.5.

The cell in Fig. 13 under hindered heat dissipation conditions showed a voltage maximum and eventually a tendency to voltage leveling at end of charge. The sister cell, which dissipated heat faster (Fig. 3, curve 4) showed sharp voltage increase and lower overcharge. The cell behavior of Fig. 13 can be explained as follows.

The cell started high plateau charge at a temperature close to ambient temperature, T_0. During charge, the cell gradually increases voltage and heat generation because of an increasing concentration of high polysulfides and shuttle current. Heat generated due to the shuttle current exceeds the heat dissipated due to the temperature gradient. Equation 26 represents the internal temperature change due to the processes described above

$$\frac{dT}{dt} = \frac{1}{mc_h}[k_S(T)q_H[S_H]V_H - \alpha(T - T_0)] \quad [26]$$

where $k_S(T)$ is the shuttle constant depending on temperature according to Eq. 24, m is the cell mass, and c_h is the cell heat capacity. At a certain temperature, the shuttle constant became high enough

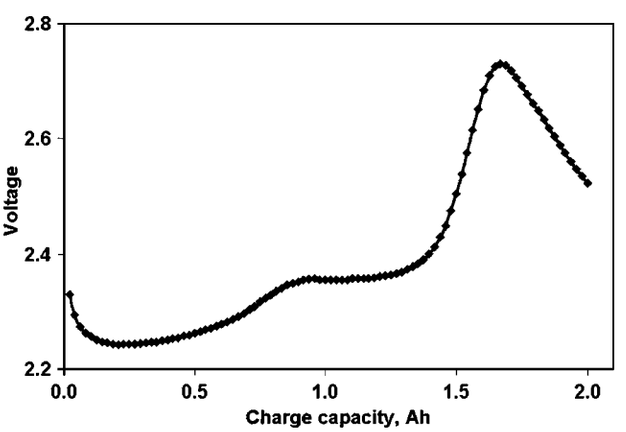

Figure 13. Experimental cell charge profile with 1.85 m salt concentration in mixture of DOL and DME electrolyte, 200 mA charge current. The cell was placed in a polyethylene bag.

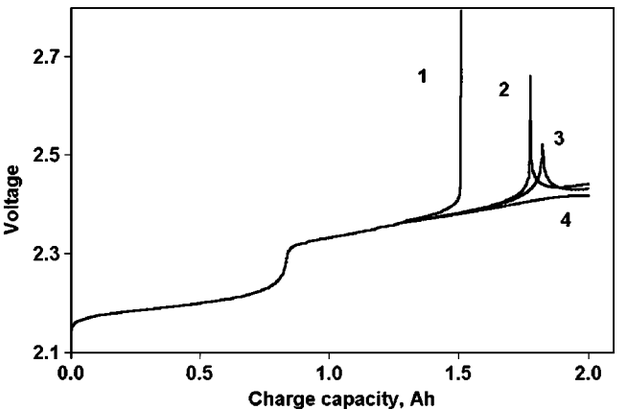

Figure 14. Simulated charge profile at different heat transfer coefficients: (1) 0.016, (2) 0.01470, (3) 0.01466, and (4) 0.01450 W K^{-1}.

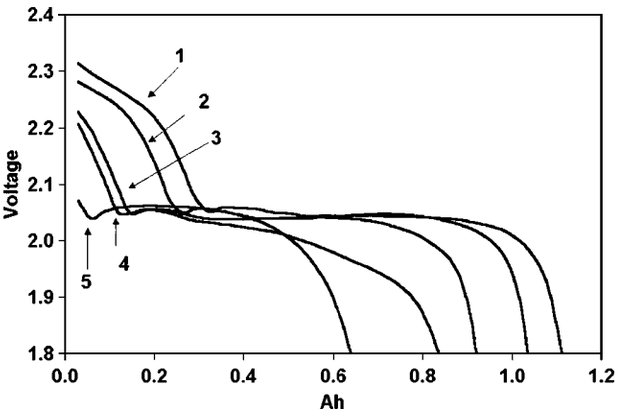

Figure 16. Discharge profiles for cell with 1.85 *m* salt $LiN(CF_3SO_2)_2$ in mixture of DOL and DME electrolyte at different storage times: (1) 0, (2) 2, (3) 4, (4) 6, and (5) 24 h.

and the shuttle current began exceeding the charge current and reduced the amount of high polysulfides, thus reducing the cell voltage. Eventually, due to continuous heat dissipation, the cell came to a steady-state condition where the shuttle current is equal to the charge current and the internal temperature stabilized.

A simulation of the charge process with dynamically changing cell internal temperature and shuttle constant is presented in Fig. 14. The lumped-heat-capacity method has been used for numerical simulations.[11] Differential shuttle equation (Eq. 5) bounded with Eq. 26 and 24 was used to describe the high polysulfides and temperature dynamic. Equation 8-10 have been used to describe the cell voltage dynamic. The cell mass was taken as 10 g, and the cell heat capacity of 1.65 J g^{-1} K^{-1} was calculated based on the heat capacities of all cell components. The simulated charge current was 200 mA.

The simulated charge profiles in Fig. 14 show a sharp voltage maximum compared with a broad maximum for the experimental cell in Fig. 12. This difference could be caused by an uneven distribution of thermal field and charge current for the experimental cell. It does not mean that the temperature or current distribution is uneven, it means that the system at a certain combination of charge and thermal parameters became extremely sensitive to minute fluctuations. The heat transfer differences for curves 2, 3, and 4 in Fig. 14 are below 1%; however, this caused a dramatic change in the charge profile shape. Such heat transfer fluctuations could be expected for a real cell because it does not have the shape of an ideal sphere and is always placed in a nonisotropic compartment.

Figure 15 represents simulations similar to those in Fig. 14 at different charge currents and a constant heat transfer coefficient of 0.01466 W K^{-1}. These simulations clearly show very high system sensitivity to current density fluctuations.

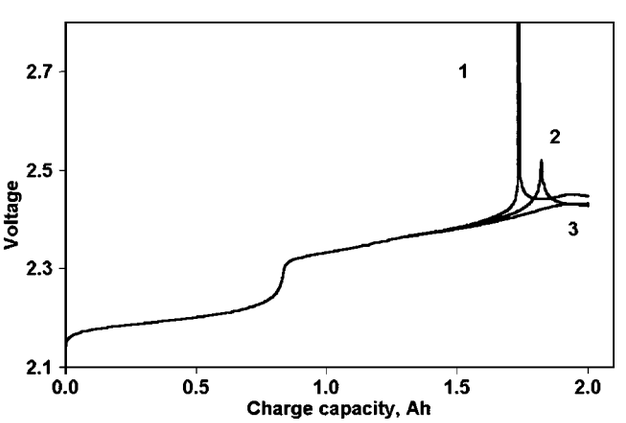

Figure 15. Simulated charge profile at different current values: (1) 201, (2) 200, and (3) 199 mA.

Shuttle and Self-Discharge

The Shuttle equation (Eq. 5) taken with current equal to zero represents cell shelf storage conditions (self-discharge process). Under shelf storage conditions, the amount of high plateau sulfur S_H has to show exponential decay with storage time t_S

$$[S_H] = [S_H^0]e^{-k/t} \quad [27]$$

If the discharge current is high enough and $f_D \ll 1$, the experimental high plateau discharge capacity is simply proportional to the remaining amount of high plateau sulfur

$$Q_H = [S_H]q_H = Q_H^0 e^{-k/t} \quad [28]$$

Q_H^0 is the starting high plateau capacity and t_S is the storage time. Equation 28 allows us to estimate the shuttle constant based on the high plateau self-discharge data.

Experimental evaluation of the high plateau self-discharge was performed with cells containing 0.5, 1.85, and 2.5 m salt electrolytes. The cells were charged at 200 mA to a voltage of 2.8 V if the charge process showed a sharp voltage increase or to total charge capacity 2000 mAh if the cell showed voltage leveling. The charged cells were stored for different times and discharged at 350 mA. As an example, Fig. 16 represents experimental cell discharge profiles stored for different times under charge conditions for 1.85 m salt concentration. For all three electrolytes, only a high plateau capacity decay was observed for a storage time range from several hours to several days. This rapid high plateau capacity fade is caused by a higher reactivity of high polysulfides Li_2S_x with $x > 4$ and has been observed in earlier papers.[1,3,5,9] The low plateau capacity was very stable for several weeks.

Experimental high plateau capacities extracted from discharge profiles and self-discharge data at 25°C are presented in Fig. 17 as a function of relative changes of high plateau discharge capacity described by Eq. 29

$$\ln\frac{Q_H}{Q_H^0} = -k_S t_S \quad [29]$$

The experimental logarithmic presentation is linear with time, consistent with Eq. 29. The slope of the curves in Fig. 17 is equal to the shuttle or self-discharge constant k_S

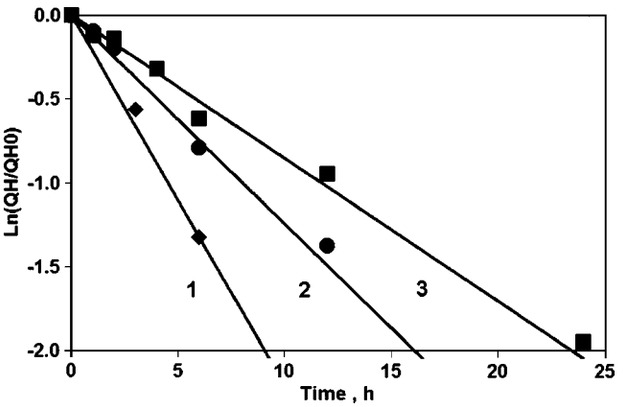

Figure 17. Experimental high plateau capacity *vs.* time for cells with different salt concentrations in mixture of DOL and DME electrolytes: (1) 0.5, (2) 1.85, and (3) 2.5 *m*.

$$\frac{d \ln Q_H}{dt_S} = -k_S \quad [30]$$

The lowest rate of self-discharge and k_S value were observed for the cells with the highest concentration of salt equal to 2.5 *m*. This trend is consistent with shuttle constant data obtained on discharge and charge current experiments for this electrolyte.

Conclusions

Consideration of the shuttle phenomenon impact on Li/S cell performance has been performed based on an application of the basic shuttle equation (Eq. 5) for various cell test conditions. Previous sections showed consistency of theoretical and experimental data. The remaining question is how experimental conditions or experimental techniques influence the shuttle constant evaluation. Table II presents shuttle constant values for three electrolytes derived from different experiments.

Different experimental techniques delivered similar k_S values for the same electrolyte. Only one significant difference was observed with the 0.5 *m* salt electrolyte for k_S at charge and self-discharge tests. Cell self-heating effects caused this difference. For the group of experiments performed with the same electrolyte, some marginal trend of shuttle constant reduction could be detected for the sequence charge-discharge-self-discharge. This trend was possibly caused by the gradual reduction of lithium surface activity while moving from charge to discharge and to self-discharge conditions. Reduction of the cell self-heating could cause a similar trend.

Table II. Shuttle constant at 25°C derived at different experimental conditions.

	Shuttle constant, k_S (h^{-1})		
	Method of k_S evaluation		
$LiN(CF_3SO_2)_2$ concentration (*m*)	High plateau *vs.* charge current	High plateau *vs.* discharge current	High plateau *vs.* storage time self-discharge
0.50	0.53	0.45	0.22
1.85	0.19	0.14	0.12
2.50	0.10	0.095	0.08

Different electrolytes demonstrated different shuttle constants. Electrolytes with higher salt concentration showed lower rates of Li corrosion with polysulfides and a lower shuttle constant. The mechanism of salt concentration influence on shuttle constant is not yet fully understood. For further understanding of this phenomenon, at least three factors should be taken into theoretical and experimental consideration: salt concentration influence on Li/electrolyte interface and on the rate of heterogeneous reaction of polysulfides with the lithium surface, salt concentration influence on the polysulfides solubility and equilibrium, and salt concentration influence on electrolyte viscosity and polysulfide mobility.

Generally, the consistency of experimental and theoretical dependencies as well as the consistency of shuttle constant values derived from different experimental techniques show that features of the charge process, discharge capacity, charge-discharge efficiency, and self-discharge are all facets of the same phenomenon.

Sion Power Corporation assisted in meeting the publication costs of this article.

References

1. R. D. Rauh, K. M. Abraham, G. F. Pearson, J. K. Surprenant, and S. B. Brummer, *J. Electrochem. Soc.*, **126**, 523 (1979).
2. R. D. Rauh, F. S. Shuker, J. M. Marston, and S. B. Brummer, *J. Inorg. Nucl. Chem.*, **39**, 1761 (1977).
3. E. Peled, Y. Sternberg, A. Gorenstein, and Y. Lavi, *J. Electrochem. Soc.*, **136**, 1621 (1989).
4. M.-Y. Chu, L. C. De Jonghe, S. J. Visco, and B. D. Katy, U.S. Pat. 6,030,720 (2000).
5. J. Shim, K. Striebel, and E. Cairns, *J. Electrochem. Soc.*, **149**, A1321 (2002).
6. Eur. Pat. EP 1 149 428 B1 (2003).
7. Y. V. Mikhaylik and J. R. Akridge, *J. Electrochem. Soc.*, **150**, A306 (2003).
8. Y. V. Mikhaylik and J. R. Akridge, Abstract 430, The Electrochemical Society Meeting Abstracts, Vol. 2003-2, Orlando, FL, Oct 12-16, 2003.
9. S. Cheon, K. Ko, J. Cho, S. Kim, E. Chin, and H. Kim, *J. Electrochem. Soc.*, **150**, A796 (2003).
10. S. Cheng and J. D. West, U.S. Pat. 6,566,006 (2003).
11. J. P. Hollman, *Heat Transfer*, 8th ed., McGraw-Hill, New York (1997).